Shifts due to neighboring resonances for microwave measurements of the $2\,^3P$ fine structure of helium

A. Marsman, M. Horbatsch, and E. A. Hessels*
Department of Physics and Astronomy, York University, Toronto, Ontario, Canada, M3J 1P3
(Received 1 June 2012; published 19 July 2012)

Quantum-mechanical interference with far-off-resonance neighboring states is found to cause systematic shifts for the measurements of the $2\,^3P$ fine-structure intervals. The shifts depend on the type of experiment used to measure the intervals. Here the shifts are calculated for measurements using a single microwave pulse and for measurements using the Ramsey method of separated oscillatory fields. The shifts are small, but are large enough to affect the continuing program of determining the fine-structure constant from a comparison between accurate experimental measurements and theoretical calculations of the interval energies. The separated-oscillatory-field shifts are found to be much smaller than the single-pulse shifts.

DOI: 10.1103/PhysRevA.86.012510 PACS number(s): 32.70.Jz, 32.80.−t

I. INTRODUCTION

In previous papers [1,2], we have shown that the line center of a resonance is shifted due to interference with a distant neighboring resonance. Those papers treated simple three- and four-level atoms, for which analytic line shapes and shifts could be derived. The analytic calculations give intuition about the size of the shifts and the scaling of these shifts, but are not directly applicable to more complicated atomic systems. In this work, we extend the analysis to a multilevel atomic system, and we also deduce the shifts that are present when using the Ramsey technique of separated oscillatory fields. We apply our analysis to the $2\,^3P$ fine-structure intervals of helium; intervals that are of direct interest for precision measurements since they can be used to determine the fine-structure constant α.

The idea of determining α from a comparison of a precise measurement and theory of the $2\,^3P$ fine structure in helium dates back to 1964, when Schwartz suggested [3] that a part-per-million determination of α might be possible if both the theory and experiment made significant advances. Since that time, large theoretical programs [4–24] and experimental programs [25–42] have made significant progress, and a determination of α to better than a part per billion (ppb) may soon be possible.

In this work, we show that interference from distant neighboring resonances shifts the line centers for the $2\,^3P$ fine-structure intervals, that the shifts are large enough to be significant for a precise determination of α, and that the magnitude of the shifts depends on both the measurement technique and on the experimental parameters used.

II. DENSITY MATRIX FORMULATION

The helium $n = 2$ triplet levels are shown in Fig. 1. A comparison between the theory and experiment for the larger $2\,^3P_2$-to-$2\,^3P_0$ (or $2\,^3P_1$-to-$2\,^3P_0$) interval allows for a precise determination of α, and a similar comparison of the smaller $2\,^3P_2$-to-$2\,^3P_1$ interval (which, because of its smaller size, is less sensitive to α) provides an independent test of the theory for the intervals.

For the present work, we consider microwave transitions between the $2\,^3P$ levels. For simplicity (and to follow the experimental technique used in [39–42]), we assume that the $2\,^3P_1 m_J = 0$ state (denoted $|1\rangle$ in Fig. 1) is initially populated (i.e., in terms of the density matrix $\rho_{11} = 1$). State $|1\rangle$ has the convenient property that it cannot decay down to the $2\,^3S_1 m_J = 0$ state (which is denoted as $|b\rangle$ in Fig. 1), and thus the population of state $|b\rangle$ remains empty ($\rho_{bb} = 0$) unless an applied microwave field drives the population out of the $|1\rangle$ state. A linearly polarized microwave field is assumed to be nearly resonant with the $2\,^3P_1 m_J = 0$-to-$2\,^3P_2 m_J = 0$ ($|1\rangle \rightarrow |2\rangle$) transition (as shown by the solid arrow in Fig. 1) and we consider the shifts that result from interference with the distant $2\,^3P_1 m_J = 0$-to-$2\,^3P_0 m_J = 0$ ($|1\rangle \rightarrow |0\rangle$) transition. Alternately, we consider a microwave field that is nearly resonant with the $|1\rangle \rightarrow |0\rangle$ transition (as shown by the dashed arrow in Fig. 1) and consider the shifts due to the distant $|1\rangle \rightarrow |2\rangle$ transition.

Microwave measurements of the $2\,^3P$ intervals can be obtained either with a single pulse of microwaves [Fig. 2(a)] or by using the Ramsey method of separated oscillatory fields (SOF), for which the atoms interact with two microwave pulses, with the pulses either in phase [Fig. 2(b)] with each other, or 180° out of phase [Fig. 2(c)]. The SOF signal is obtained by subtracting the signal obtained using Fig. 2(c) from that obtained using Fig. 2(b).

In the magnetic dipole approximation, $U(t) = -\vec{\mu} \cdot \vec{B}(t)$ couples state $|1\rangle$ to both $|2\rangle$ and $|0\rangle$. Here, $\vec{B}(t) = \vec{B}_0 g(t) \cos(\omega t + \phi)$, with [for the cases of Figs. 2(a), 2(b), and 2(c), respectively] $g_a(t) = \sigma_D(t)$ and $g_{b,c}(t) = [\sigma_D(t) \pm \sigma_D(t - T)]$, where $\sigma_D(t)$ is a pulse of unit amplitude and with FWHM duration D.

The density matrix equations for determining the population in states $|1\rangle$, $|2\rangle$, $|0\rangle$, and $|b\rangle$ for this system are [43,44]

$$\dot{\rho}_{11} = iV_{12}\rho_{12} - iV_{21}\rho_{21} + iV_{10}\rho_{10} - iV_{01}\rho_{01} - \gamma_1\rho_{11} - \frac{\gamma_{10}}{2}(\rho_{10} + \rho_{01}) - \frac{\gamma_{12}}{2}(\rho_{12} + \rho_{21}), \tag{1a}$$

$$\dot{\rho}_{12} = iV_{21}(\rho_{11} - \rho_{22}) - \left(\frac{\gamma_1 + \gamma_2}{2} - i\omega_{21}\right)\rho_{12} - iV_{01}\rho_{02} - \frac{\gamma_{20}}{2}\rho_{10} - \frac{\gamma_{12}}{2}(\rho_{11} + \rho_{22}) - \frac{\gamma_{10}}{2}\rho_{02}, \tag{1b}$$

*hessels@yorku.ca

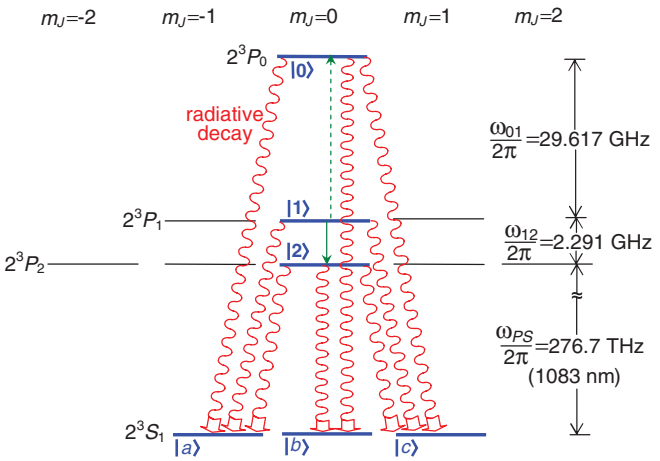

FIG. 1. (Color online) The $n = 2$ triplet energy levels of helium. For this work the population is assumed to start in the $|1\rangle$ state and an applied microwave field either drives the $|1\rangle \rightarrow |2\rangle$ transition (solid arrow) or the $|1\rangle \rightarrow |0\rangle$ transition (dashed arrow). The allowed radiative decay paths from states $|1\rangle$, $|2\rangle$, and $|0\rangle$ are indicated. When driving one of the resonances (the solid arrow or the dashed arrow), a far-off-resonant transition amplitude from the other resonance causes a shift in the measured line center.

$$\dot{\rho}_{22} = iV_{21}\rho_{21} - iV_{12}\rho_{12} - \gamma_2\rho_{22} - \frac{\gamma_{20}}{2}(\rho_{20} + \rho_{02}) - \frac{\gamma_{12}}{2}(\rho_{21} + \rho_{12}), \tag{1c}$$

$$\dot{\rho}_{10} = iV_{01}(\rho_{11} - \rho_{00}) - iV_{21}\rho_{20} - \left(\frac{\gamma_1 + \gamma_0}{2} - i\omega_{01}\right)\rho_{10} - \frac{\gamma_{20}}{2}\rho_{12} - \frac{\gamma_{10}}{2}(\rho_{11} + \rho_{00}) - \frac{\gamma_{12}}{2}\rho_{20}, \tag{1d}$$

$$\dot{\rho}_{20} = iV_{01}\rho_{21} - iV_{12}\rho_{10} - \left(\frac{\gamma_2 + \gamma_0}{2} - i\omega_{02}\right)\rho_{20} - \frac{\gamma_{20}}{2}(\rho_{22} + \rho_{00}) - \frac{\gamma_{12}}{2}\rho_{10} - \frac{\gamma_{10}}{2}\rho_{21}, \tag{1e}$$

$$\dot{\rho}_{00} = iV_{01}\rho_{01} - iV_{10}\rho_{10} - \gamma_0\rho_{00} - \frac{\gamma_{20}}{2}(\rho_{02} + \rho_{20}) - \frac{\gamma_{10}}{2}(\rho_{01} + \rho_{10}), \tag{1f}$$

$$\dot{\rho}_{bb} = \gamma_{1\to b}\rho_{11} + \gamma_{2\to b}\rho_{22} + \gamma_{0\to b}\rho_{00} + \gamma_{12\to b}(\rho_{21} + \rho_{12}) + \gamma_{10\to b}(\rho_{01} + \rho_{10}) + \gamma_{20\to b}(\rho_{02} + \rho_{20}), \tag{1g}$$

where $V_{ij} = \langle i|U(t)|j\rangle/\hbar$; and $\tau_1 = \gamma_1^{-1}$, $\tau_2 = \gamma_2^{-1}$, and $\tau_0 = \gamma_0^{-1}$ are the lifetimes of states $|1\rangle$, $|2\rangle$, and $|0\rangle$. In terms of the partial decay rates of the radiative decay paths shown in Fig. 1, $\gamma_i = \gamma_{i\to a} + \gamma_{i\to b} + \gamma_{i\to c}$. Similarly, we define $\gamma_{ij} = \gamma_{ij\to a} + \gamma_{ij\to b} + \gamma_{ij\to c}$, where (in the electric dipole approximation)

$$\gamma_{i\to b} = \frac{4e^2|\omega_{PS}|^3}{3\hbar c^3}\langle i|\vec{r}\,|b\rangle \cdot \langle b|\vec{r}\,|i\rangle, \tag{2a}$$

and

$$\gamma_{ij\to b} = \frac{4e^2|\omega_{PS}|^3}{3\hbar c^3}\langle i|\vec{r}\,|b\rangle \cdot \langle b|\vec{r}\,|j\rangle. \tag{2b}$$

Since $\omega_{PS} \gg \omega_{12}, \omega_{01}$ (as shown in Fig. 1), $\gamma_1 = \gamma_2 = \gamma_0$, and all are equal to $\gamma = 1/\tau$, where $\tau = 97.9$ ns. Also, due to cancellations, $\gamma_{12} = \gamma_{10} = \gamma_{20} = 0$, and, due to a zero dipole matrix element, $\gamma_{1\to b} = \gamma_{12\to b} = \gamma_{10\to b} = 0$. From the electric-dipole matrix elements, one obtains $\gamma_{2\to b} = 2\gamma/3$, $\gamma_{0\to b} = \gamma/3$ and $\gamma_{20\to b} = -\sqrt{2}\gamma/3$. The nonzero $\gamma_{20\to b}$ term in Eq. (1) results directly from quantum-mechanical interference of the radiative decay.

Furthermore, from the ratio of the magnetic dipole matrix elements, $V_{10} = V_{01} \equiv V$ and $V_{21} = V_{12} = V/\sqrt{2}$, where $V = V_0 g(t)\cos(\omega t + \phi)$, with $V_0 = (\mu_B/\hbar)\sqrt{2/3}B_0$. Thus, Eq. (1) simplifies to

$$\dot{\rho}_{11} = \frac{iV}{\sqrt{2}}(\rho_{12} - \rho_{21}) + iV(\rho_{10} - \rho_{01}) - \gamma\rho_{11}, \tag{3a}$$

$$\dot{\rho}_{12} = \frac{iV}{\sqrt{2}}(\rho_{11} - \rho_{22}) - (\gamma - i\omega_{21})\rho_{12} - iV\rho_{02}, \tag{3b}$$

$$\dot{\rho}_{22} = \frac{iV}{\sqrt{2}}(\rho_{21} - \rho_{12}) - \gamma\rho_{22}, \tag{3c}$$

$$\dot{\rho}_{10} = iV(\rho_{11} - \rho_{00}) - \frac{iV}{\sqrt{2}}\rho_{20} - (\gamma - i\omega_{01})\rho_{10}, \tag{3d}$$

$$\dot{\rho}_{20} = iV\rho_{21} - \frac{iV}{\sqrt{2}}\rho_{10} - (\gamma - i\omega_{02})\rho_{20}, \tag{3e}$$

$$\dot{\rho}_{00} = iV(\rho_{01} - \rho_{10}) - \gamma\rho_{00}, \tag{3f}$$

$$\dot{\rho}_{bb} = \frac{2\gamma}{3}\rho_{22} + \frac{\gamma}{3}\rho_{00} - \frac{\sqrt{2}\gamma}{3}(\rho_{02} + \rho_{20}). \tag{3g}$$

Note that neither Eq. (1) nor Eq. (3) use the rotating-wave approximation and that V in Eq. (3) is time dependent.

Equation (3), along with the complex conjugate equations for $\dot{\rho}_{21}$, $\dot{\rho}_{02}$, and $\dot{\rho}_{01}$, can be used to obtain ρ_{11}, ρ_{22}, ρ_{00}, and ρ_{bb} (i.e., the populations of states $|1\rangle$, $|2\rangle$, $|0\rangle$, and $|b\rangle$). The other density matrix equations for $\dot{\rho}_{ai}$, $\dot{\rho}_{bi}$, $\dot{\rho}_{ci}$, $\dot{\rho}_{ia}$, $\dot{\rho}_{ib}$, and $\dot{\rho}_{ic}$ are not needed since these ρ_{jk} do not appear on the right-hand side of Eq. (1), and therefore are decoupled from the system of equations given in Eq. (3).

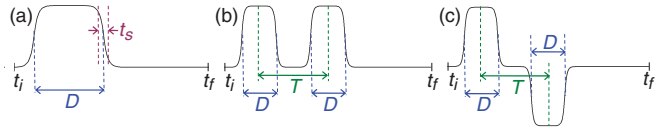

FIG. 2. (Color online) Timing for the microwave pulses. (a) A single microwave pulse is considered. (b, c) The in-phase and 180°-out-of-phase cases for two pulses are represented. The difference of signal obtained in (b) and (c) allows for subnatural line widths using the Ramsey SOF technique. A switching time of $t_s = 1$ ns is included in the calculations.

III. NUMERICAL INTEGRATION

Equations (3a) through (3g) are numerically integrated using a fourth-order Runge-Kutta method. The value of ρ_{bb} at $t = t_f$ of Fig. 2 is a direct measure of the probability that a microwave transition has been made. This method of detecting microwave transitions follows the experimental technique used in [39–42]. The numerical integrations are repeated for a range of frequencies near the resonance to trace out the resonance line shape. These line shapes are then fit to determine the shifts caused by the distant neighboring resonance. The integrations are started at a time t_i that is 50 ns

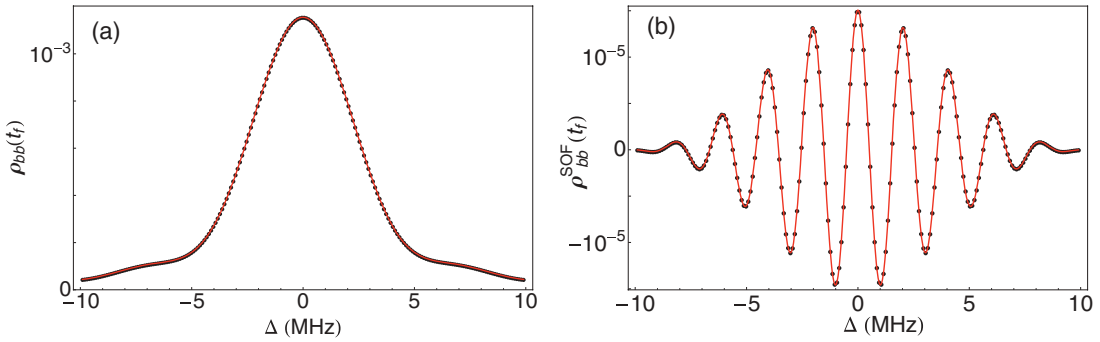

FIG. 3. (Color online) Line shapes of the $|1\rangle \rightarrow |2\rangle$ resonance obtained from numerical integrations for (a) a single microwave pulse with a duration $D = 200$ ns, and for (b) SOF with two microwave pulses of $D = 100$ ns, separated by $T = 500$ ns. These line shapes are for a microwave magnetic field amplitude of $B_0 = 0.2$ gauss and show that the initially empty $|b\rangle$ state of Fig. 1 is populated when the microwave transition is driven. The fits (solid lines) are obtained using Eqs. (4) and (5). The fits are used to determine small shifts in the resonance line centers, as shown in Fig. 4 and Tables I and II.

before the start of the first microwave pulse and continued until a time t_f that is 500 ns after the end of the last pulse (see Fig. 2). The 500 ns allows almost all of the 2^3P atoms to decay back down to the 2^3S states. As indicated in Fig. 2, the microwave pulses used have a time constant t_s for turn on and turn off. The shifts obtained are found to be essentially independent of t_s for t_s between 1 and 10 ns, which corresponds to experimentally realizable turn-on and turn-off times, and $t_s = 1$ ns is used for all integrations presented here. For much shorter t_s, the high frequencies associated with the sudden turn on and turn off, modify the shifts by approximately 10%.

The numerical integrations use 30-fs time steps to accurately integrate through the approximately 30-GHz frequencies of the applied microwave field and the complex phase factor of the atomic wave function. The numerical integrations are checked by using both higher-precision arithmetic and shorter time steps and further checked by comparing to numerical integrations using a Runge-Kutta-Fehlberg method.

Sample line shapes obtained from these integrations are shown in Fig. 3, where the final $|b\rangle$ state population $[\rho_{bb}(t_f)]$ is shown for an initial population in the $|1\rangle$ state $[\rho_{bb}(t_i) = 1]$. In Fig. 3(a), a line shape is shown for a single microwave pulse of duration $D = 200$ ns. Figure 3(b) shows the Ramsey SOF line shape obtained from two microwave pulses of duration $D = 100$ ns that are separated by a time $T = 500$ ns. This line shape is obtained by subtracting the line shape obtained from integrations using the 180°-out-of-phase microwave pulses of Fig. 2(c) from the line shape obtained using the in-phase microwave pulses of Fig. 2(b).

IV. SHIFTS

To determine the shifts of the numerically generated line shapes (such as those shown in Fig. 3), least-squares fits are performed. The fit functions used for a single microwave pulse and for SOF are (respectively)

$$\rho_{bb} = C \int_{t=0}^{\infty} \left[\frac{s(t_L)}{\Delta}\right]^2 e^{-\gamma t} dt, \tag{4}$$

and

$$\rho_{bb}^{\mathrm{SOF}} = C \int_{t=0}^{\infty} s(D) s(t_L) f(t_L) e^{-\gamma t} \cos(\Delta \mathcal{T}) dt, \tag{5}$$

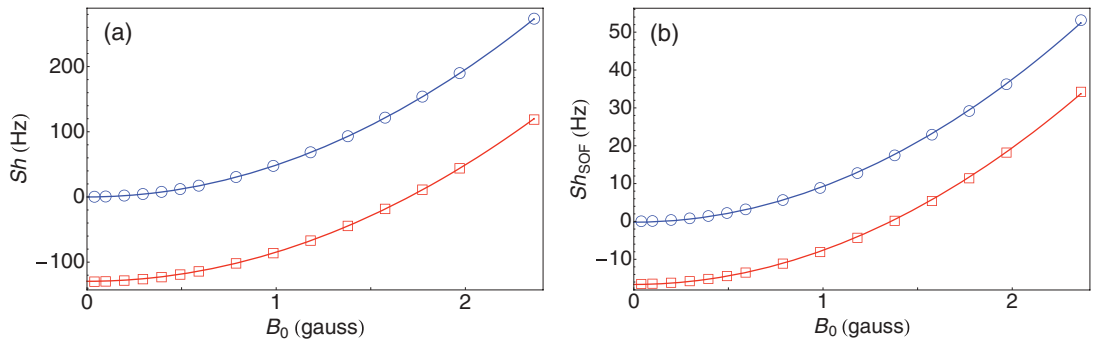

FIG. 4. (Color online) Shifts of the $|1\rangle \rightarrow |2\rangle$ resonance versus microwave field strength. The shifts for (a) a single microwave pulse with a duration $D = 200$ ns and for (b) SOF with two microwave pulses of $D = 100$ ns, separated by $T = 500$ ns, are obtained by fits similar to those shown in Fig. 3. On each plot, the squares represent the full shift and the circles the shifts that would result in the absence of the $\gamma_{20\rightarrow b}$ interference term in Eq. (1). The quadratic fits shown [Eq. (6)] are used to extrapolate to zero microwave power.

where

$$f(t) = s(D)s(t) - c(D)c(t) + \tan(\Delta\mathcal{T})s(D+t),$$

with

$$s(t) = \frac{\sin\left(\sqrt{\Delta^2 + V_0^2}\,t/2\right)}{\sqrt{\Delta^2 + V_0^2}/\Delta}, \quad c(t) = \cos\left(\sqrt{\Delta^2 + V_0^2}\,\frac{t}{2}\right),$$

$\mathcal{T} = T - D$, $\Delta = f - f_0$, $f = \omega/2\pi$, and t_L being the lesser of t and D [i.e., $t_L = \min(t, D)$]. Equations (4) and (5) are the exact line shapes in the rotating-wave approximation, assuming that the fields turn on and off suddenly and ignoring the effects of nonresonant states. In the fits (examples of which are shown by the solid lines in Fig. 3), only f_0 of Eqs. (4) and (5) is allowed to float, and the fit value for f_0 determines the shift caused by the quantum-mechanical interference (and also the ac shift). Alternate methods for determining the shifts based on the positions and slopes at the half maximum positions in Fig. 3(a) and of the zero-crossing points in Fig. 3(b) lead to nearly identical shifts. The very small differences between shifts obtained from the different methods is due to very small distortions in the line shape caused by the $\gamma_{20\to b}$ interference term.

The shifts obtained by the fits are shown in Fig. 4. The circles in the figure show the shifts that result when the $\gamma_{20\to b}$ interference term in Eq. (1) is excluded. These shifts scale as the square of the microwave field strength due to the expected ac power shifts, and extrapolate to zero for zero field intensity. The square symbols in the plots represent the full shift (including the $\gamma_{20\to b}$ interference term). These shifts do not extrapolate to zero, but rather have the form

$$Sh = Sh^{(0)} + kB_0^2, \tag{6}$$

where B_0 is the amplitude of the applied microwave field, k is the ac shift rate, and $Sh^{(0)}$ is the remaining shift at zero intensity. The shifts $Sh^{(0)}$ are listed in Tables I and II and are almost identical for the $2\,^3P_1$-to-$2\,^3P_0$ and $2\,^3P_1$-to-$2\,^3P_2$ intervals. For the single-pulse shifts (Table I), the shifts are approximately inversely proportional to the pulse duration D, while for the SOF measurements (Table II), the much smaller shifts are approximately inversely proportional to the pulse separation T.

TABLE I. Frequency shifts [extrapolated to zero microwave intensity using Eq. (6), as shown in Fig. 4(a)] for helium $2\,^3P_1$-to-$2\,^3P_0$ ($|1\rangle \to |0\rangle$) and $2\,^3P_1$-to-$2\,^3P_2$ ($|1\rangle \to |2\rangle$) single-microwave-pulse transitions.

	$Sh^{(0)}_{\text{single-pulse}}$ (Hz)	
D (ns)	$\|1\rangle \to \|0\rangle$	$\|1\rangle \to \|2\rangle$
50	−429	−429
100	−224	−224
200	−129	−129
400	−87	−88
800	−82	−82

TABLE II. Frequency shifts [extrapolated to zero microwave intensity using Eq. (6), as shown in Fig. 4(b)] for helium $2\,^3P_1$-to-$2\,^3P_0$ ($|1\rangle \to |0\rangle$) and $2\,^3P_1$-to-$2\,^3P_2$ ($|1\rangle \to |2\rangle$) SOF transitions.

		$Sh^{(0)}_{\text{SOF}}$ (Hz)	
D (ns)	T (ns)	$\|1\rangle \to \|0\rangle$	$\|1\rangle \to \|2\rangle$
50	200	−41	−41
50	300	−27	−27
50	400	−20	−20
50	500	−16	−16
50	600	−14	−14
50	800	−10	−10
100	300	−27	−28
100	400	−20	−21
100	500	−16	−17
100	600	−14	−14
100	800	−10	−10
150	400	−21	−22
150	500	−16	−17
150	600	−14	−14
150	800	−10	−11

V. CONCLUSION

Although the shifts shown in Tables I and II are small, microwave measurements of the intervals are now approaching an accuracy where the shifts will need to be considered. The most accurate single-pulse microwave measurements [40,41] have uncertainties of 900 and 1400 Hz. These measurements have a pulse duration D determined by the travel time through the microwave region. Since this D is typically 950 and 1700 ns for the two measurements, it can be seen from Table I that the interference corrections are less than 10% of the measurement uncertainties. The most accurate SOF measurement [42] of the helium $2\,^3P$ fine structure has an uncertainty of 350 Hz. This measurement uses $D = 50$, 100, and 150 ns and $T = 300$, 400, 500, and 600 ns. From Table II, it is evident that the corrections that need to be applied are again less than 10% of the measurement uncertainty. The corrections shown in the $|1\rangle \to |0\rangle$ columns of Tables I and II indicate shifts of 0.5 to 15 ppb of the 29.6 GHz interval and these will be important in the anticipated next generation of microwave measurements and are a necessary step towards a ppb determination of α from helium $2\,^3P$ fine structure.

Interference shifts similar to those calculated here are also expected to be significant for other precision measurements, and calculations similar to those presented here should be applied to these other measurements to ensure that this systematic correction is properly applied.

ACKNOWLEDGMENTS

This work is supported by NSERC, CRC, ORF, CFI, and NIST, and the computations were done using SHARCNET.

[1] M. Horbatsch and E. A. Hessels, Phys. Rev. A **82**, 052519 (2010).
[2] M. Horbatsch and E. A. Hessels, Phys. Rev. A **84**, 032508 (2011).
[3] C. Schwartz, Phys. Rev. **134**, A1181 (1964).
[4] B. Schiff, C. L. Pekeris, and H. Lifson, Phys. Rev. **137**, A1672 (1965).
[5] K. Y. Kim, Phys. Rev. **140**, A1498 (1965).
[6] L. Hambro, Phys. Rev. A **5**, 2027 (1972).
[7] L. Hambro, Phys. Rev. A **6**, 865 (1972).
[8] L. Hambro, Phys. Rev. A **7**, 479 (1973).
[9] M. Douglas and N. M. Kroll, Ann. Phys. (NY) **82**, 89 (1974).
[10] J. Daley, M. Douglas, L. Hambro, and N. M. Kroll, Phys. Rev. Lett. **29**, 12 (1972).
[11] M. L. Lewis and P. H. Serafino, Phys. Rev. A **18**, 867 (1978).
[12] Z.-C. Yan and G. W. F. Drake, Phys. Rev. Lett. **74**, 4791 (1995).
[13] T. Zhang, Phys. Rev. A **54**, 1252 (1996).
[14] T. Zhang, Phys. Rev. A **53**, 3896 (1996).
[15] T. Zhang, Z.-C. Yan, and G. W. F. Drake, Phys. Rev. Lett. **77**, 1715 (1996).
[16] G. W. F. Drake, Can. J. Phys. **80**, 1195 (2002).
[17] K. Pachucki and J. Sapirstein, J. Phys. B **33**, 5297 (2000).
[18] K. Pachucki and J. Sapirstein, J. Phys. B **36**, 803 (2003).
[19] J. Sapirstein, J. Phys. B **43**, 074015 (2010).
[20] K. Pachucki, J. Phys. B **32**, 137 (1999).
[21] K. Pachucki, Phys. Rev. Lett. **97**, 013002 (2006).
[22] K. Pachucki and V. A. Yerokhin, Phys. Rev. A **79**, 062516 (2009).
[23] K. Pachucki and V. A. Yerokhin, Phys. Rev. A **80**, 019902(E) (2009).
[24] K. Pachucki and V. A. Yerokhin, Phys. Rev. Lett. **104**, 070403 (2010).
[25] F. M. J. Pichanick, R. D. Swift, C. E. Johnson, and V. W. Hughes, Phys. Rev. **169**, 55 (1968).
[26] A. Kponou, V. W. Hughes, C. E. Johnson, S. A. Lewis, and F. M. J. Pichanick, Phys. Rev. Lett. **26**, 1613 (1971).
[27] A. Kponou, V. W. Hughes, C. E. Johnson, S. A. Lewis, and F. M. J. Pichanick, Phys. Rev. A **24**, 264 (1981).
[28] W. Frieze, E. A. Hinds, V. W. Hughes, and F. M. J. Pichanick, Phys. Rev. A **24**, 279 (1981).
[29] D. Shiner, R. Dixson, and P. Zhao, Phys. Rev. Lett. **72**, 1802 (1994).
[30] D. L. Shiner and D. R, IEEE Trans. Instr. Meas. **44**, 518 (1995).
[31] J. Castillega, D. Livingston, A. Sanders, and D. Shiner, Phys. Rev. Lett. **84**, 4321 (2000).
[32] M. Smiciklas and D. Shiner, Phys. Rev. Lett. **105**, 123001 (2010).
[33] M. Prevedelli, P. Cancio, G. G, F. S. Pavone, and M. Inguscio, Opt. Comm. **125**, 231 (1996).
[34] F. Minardi, G. Bianchini, P. C. Pastor, G. Giusfredi, F. S. Pavone, and M. Inguscio, Phys. Rev. Lett. **82**, 1112 (1999).
[35] P. C. Pastor, G. Giusfredi, P. DeNatale, G. Hagel, C. de Mauro, and M. Inguscio, Phys. Rev. Lett. **92**, 023001 (2004).
[36] P. C. Pastor, G. Giusfredi, P. DeNatale, G. Hagel, C. de Mauro, and M. Inguscio, Phys. Rev. Lett. **97**, 139903(E) (2006).
[37] G. Giusfredi, P. C. Pastor, P. DeNatale, D. Mazzotti, C. D. Mauro, L. Fallani, G. Hagel, V. Krachmalnicoff, and M. Inguscio, Can. J. Phys. **83**, 301 (2005).
[38] T. Zelevinsky, D. Farkas, and G. Gabrielse, Phys. Rev. Lett. **95**, 203001 (2005).
[39] C. H. Storry and E. A. Hessels, Phys. Rev. A **58**, 8R (1998).
[40] C. H. Storry, M. C. George, and E. A. Hessels, Phys. Rev. Lett. **84**, 3274 (2000).
[41] M. C. George, L. D. Lombardi, and E. A. Hessels, Phys. Rev. Lett. **87**, 173002 (2001).
[42] J. S. Borbely, M. C. George, L. D. Lombardi, M. Weel, D. W. Fitzakerley, and E. A. Hessels, Phys. Rev. A **79**, 060503 (2009).
[43] D. A. Cardimona, M. G. Raymer, and C. R. Stroud Jr., J. Phys. B: At. Mol. Opt. Phys. **15**, 55 (1982).
[44] D. A. Cardimona and C. R. Stroud, Phys. Rev. A **27**, 2456 (1983).